Supplementary Information (SI) for Journal of Materials Chemistry A.
This journal is © The Royal Society of Chemistry 2025

Supplementary Information

Thermal Cycling Tuning Photoelectric Conversion in Hybrid Perovskites

Shengjian Qin[1,2], Hang Su[1,2], Yinan Jiao[2], Jiale Meng[2], Jiayu Song[1,2], Jinjin Zhao[1,*], Jian Lu[3,*]

[1] Hebei Technology Innovation Center for Energy Conversion Materials and Devices, Hebei Key Laboratory of Inorganic Nanomaterials, Engineering Research Center of Thin Film Solar Cell Materials and Devices, Hebei Province, College of Chemistry and Materials Science, Hebei Normal University, Shijiazhuang, Hebei, 050024, China

[2] School of Materials Science and Engineering, Shijiazhuang Tiedao University, Shijiazhuang 050043, China

[3] City U-Shenzhen Futian Research Institute, Shenzhen, 518045, China, Department of Mechanical Engineering, City University of Hong Kong, Hong Kong, China, Hong Kong Branch of National Precious Metals Material Engineering Research Centre, City University of Hong Kong, Hong Kong, China, Department of Materials Science and Engineering, City University of Hong Kong, Hong Kong, China, Centre for Advanced Structural Materials, City University of Hong Kong Shenzhen Research Institute, Greater Bay Joint Division, Shenyang National Laboratory for Materials Science, Shenzhen, China

[*] Corresponding author: jinjinzhao2012@163.com; cengdean@cityu.edu.hk

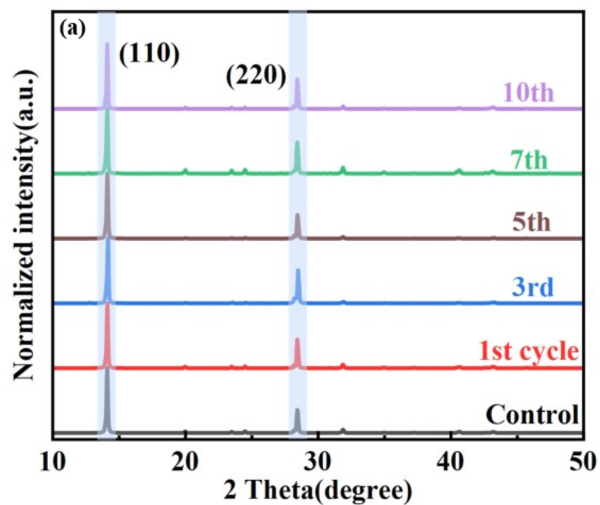

Figure S1. XRD patterns of perovskite films after RT-thermal cycling.

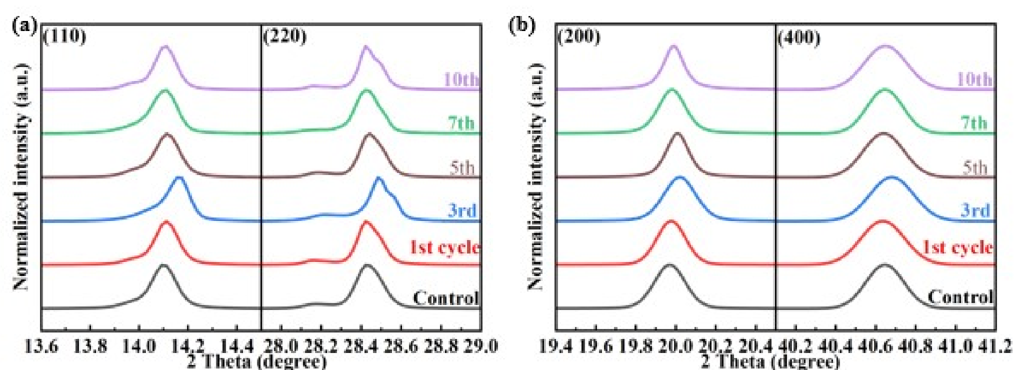

Figure S2. (a) Magnified (110) and (220) diffraction peaks. (b) Magnified (200) and (400) peaks.

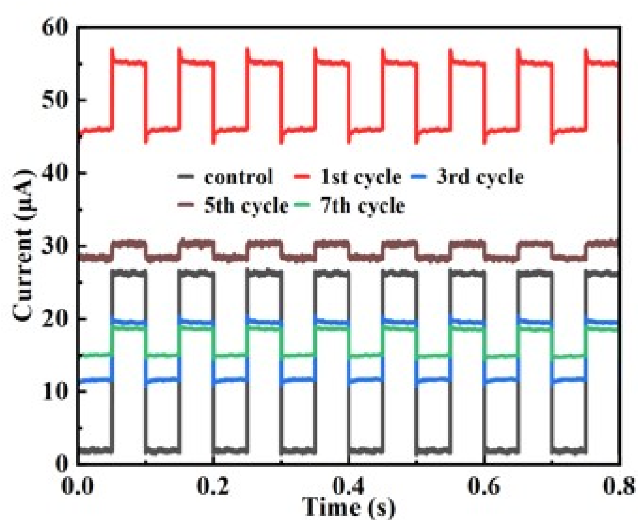

Figure S3. Current responses of the perovskite films under pulse bias voltage and light.

FIB-DIC stress characterization

Small holes with a diameter about 150 nm are milled with FIB to track the displacements of points at sample surface. A ring core with a diameter of approximately 9 μm is milled into the sample surface in a step-wise fashion by using the FIB. In between the milling steps, high resolution SEM images are acquired. This process is terminated at the milling depth which guarantees complete strain relief. As the FIB milling progresses towards greater depths, the relief strain saturates and reaches a constant value. The elastic strain relief in the central material island could be expressed by:

$$f\left(\varepsilon_1^{\infty},z\right) = 1.12\Delta\varepsilon_1^{\infty}\frac{z}{1+z}\left(1+\frac{2}{1+z^2}\right) \quad (1)$$

$$f\left(\varepsilon_2^{\infty},z\right) = 1.12\Delta\varepsilon_2^{\infty}\frac{z}{1+z}\left(1+\frac{2}{1+z^2}\right) \quad (2)$$

where ε_1^{∞} and ε_2^{∞} are the complete elastic strain relief value along x and y axis, z=(h/0.42D) (h is milling depth; D is diameter of ring core). The local resolution of residual strain versus milling depth could be reconstructed as:

$$e\left(\frac{h}{D}\right) = \int_0^{\frac{h}{D}} F\left(\frac{z}{D}\right)\varepsilon^*(z)\,d\left(\frac{z}{D}\right) \quad (3)$$

where h/D is the normalized depth with respect to the ring core diameter D. z is the eigenstrain dependent depth $\varepsilon^*(z)$, $F\left(\frac{z}{D}\right)$ is a single variable influence function describing the incremental contribution to the surface strain relief from eigenstrain. To obtain the local depth-resolved eigenstrain distribution, equation (3) can be obtained with respect to h/D via differentiation:

$$\varepsilon^*\left(\frac{h}{D}\right) = \frac{\dfrac{de\left(\frac{h}{D}\right)}{d\left(\frac{h}{D}\right)}}{F\left(\frac{h}{D}\right)} \quad (4)$$

The depth resolved in plane strain can then be calculated as ε=-ε*. If three 45° equally spaced in-plane strain reliefs are monitored throughout the milling, the strain gage rosette theory can be used. These incremental strain reliefs are named as $\Delta e_{0°,}$, $\Delta e_{45°,i}$ and $\Delta e_{90°,i}$, which are calculated through monitor the distance between holes in Figure 3d. Therefore, at each increment of the milling i, the principal strain relief ($\Delta e_{1,}$, $\Delta e_{2,i}$) can be obtained as:

$$\Delta e_{1,i} = \frac{(\Delta e_{0°,i} + \Delta e_{90°,i})}{2} + \sqrt{\frac{(\Delta e_{0°,i} - \Delta e_{45°,i})^2}{2} + \frac{(\Delta e_{90°,i} - \Delta e_{45°,i})^2}{2}}$$

(5)

$$\Delta e_{1,i} = \frac{(\Delta e_{0°,i} + \Delta e_{90°,i})}{2} + \sqrt{\frac{(\Delta e_{0°,i} - \Delta e_{45°,i})^2}{2} + \frac{(\Delta e_{90°,i} - \Delta e_{45°,i})^2}{2}}$$

(6)

At each milling step i, the isotropic strain ($\Delta e_{H,i}$) and shear strain ($\Delta e_{D,i}$) could be expressed by:

$$\Delta e_{H,i} = \frac{(\Delta e_{1,i} + \Delta e_{2,i})}{2} \quad (7)$$

$$\Delta e_{D,i} = \frac{(\Delta e_{1,i} - \Delta e_{2,i})}{2} \quad (8)$$

The principal elastic residual strains can then be obtained as:

$$\varepsilon_{1,i} = -\frac{\Delta e_{H,i}}{F_{H,i}} - \frac{\Delta e_{D,i}}{F_{D,i}} \quad (9)$$

$$\varepsilon_{2,i} = -\frac{\Delta e_{H,i}}{F_{H,i}} + \frac{\Delta e_{D,i}}{F_{D,i}} \quad (10)$$

where F_H and F_D are the influence functions respectively for the hydrostatic and deviatoric parts. The residual stresses in the two principal directions can be calculated using Hooke's law:

$$\sigma_{1,i} = \frac{E}{1 - \vartheta^2}(\varepsilon_{1,i} + \vartheta\varepsilon_{2,i}) \quad (11)$$

$$\sigma_{2,i} = \frac{E}{1 - \vartheta^2}(\varepsilon_{2,i} + \vartheta\varepsilon_{1,i}) \quad (12)$$

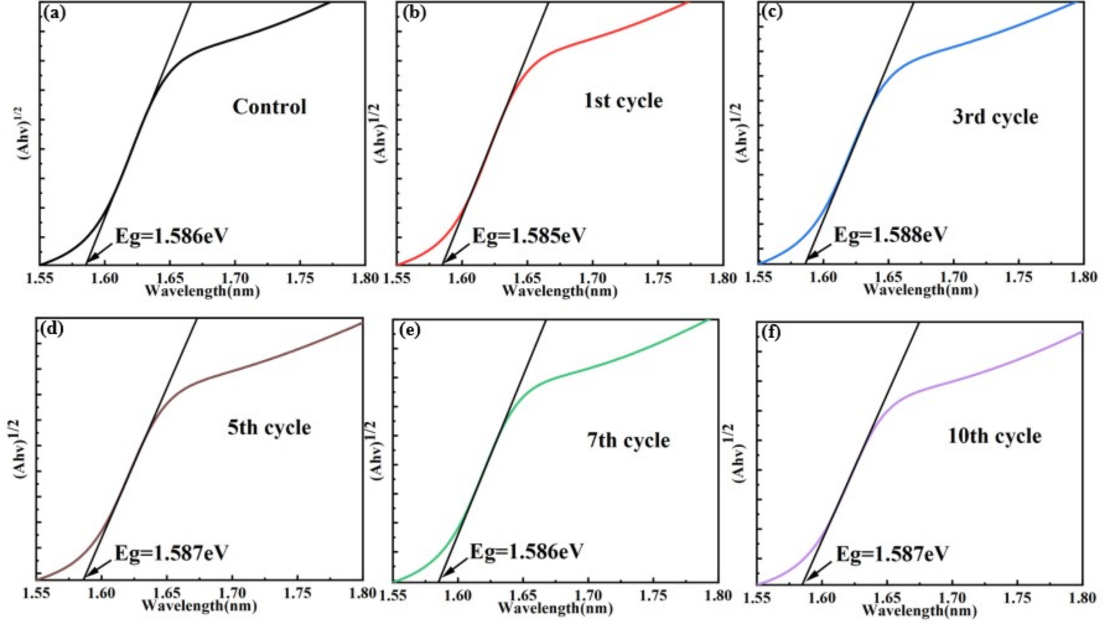

Figure S4. Band gaps calculated from the UV-vis spectroscopy absorption peak of the $MAPbI_3$ perovskite films after RT-thermal cycling.

Fitting of photoluminescence (PL) spectrum

For a direct band gap semiconductor with a parabolic band edge including both organic and inorganic perovskites[1, 2], the PL intensity could be modeled. The band-to-band radiative recombination is given by [3, 4]:

$$I_{PL}^{b}(\hbar\omega) = \begin{cases} A(\hbar\omega)^2(\hbar\omega - E_g)^{\frac{1}{2}}\exp\left(-\frac{\hbar\omega - E_g}{k_B T_e}\right) \text{if } \hbar\omega > E_g \\ 0 \text{ if } \hbar\omega < E_g \end{cases} \quad (13)$$

where $I_{PL}^{b}(\hbar\omega)$ is the PL intensity from the band-to-band transition, $\hbar\omega$ is the energy of the emitted photon, E_g is the band gap energy of the materials, T_e is the effective temperature of the material, k_B is the Boltzmann constant, A is a proportionality parameter. According to Eq. (1), the luminescence intensity should be equal to zero for and energy lower than E_g. At room temperature, there is always light emitted with energy lower than the band gap energy. This phenomenon can be explained by the existence of states close to the band-edges induced by defects, or by fluctuations in the semi-conductor stoichiometry, or linked to bound excitons. These shallow states in the band gap are suspected to be at the origin of the Urbach tail, observed close to the optical absorption edge of semi-conductors. The light intensity corresponding to

the emission of these photons is expressed by[3, 4]:

$$I_{PL}^{e}(\hbar\omega) = \begin{cases} 0 \text{ if } \hbar\omega > E_g \\ \frac{N_e}{E_0}\exp\left(-\frac{\hbar\omega - E_g}{k_B T_e}\right) \text{if } \hbar\omega < E_g \end{cases} \tag{14}$$

where $I_{PL}^{e}(\hbar\omega)$ is the below-gap luminescence intensity, N_e is a parameter proportional to the density of states, E_0 reflects the extension of the states in the band gap. The PL spectrum for an intrinsic direct band gap semiconductor can therefore be give by:

$$I_{PL}(\hbar\omega) = I_{PL}^{b}(\hbar\omega) + I_{PL}^{e}(\hbar\omega) \tag{15}$$

where A, E_g, T_e, N_e, and E_0 are taken as fitting parameters.

Calculation of Urbach energy (E_U)

Urbach tail is the broadening effect of semiconductor band edges related to the thermal and inherent lattice disorder[5, 6]. The band edge broadening is quantified by the Urbach energy (E_u), which can be derived from the slope of the linear exponential regime[7, 8]:

$$\alpha = \alpha_0 \exp\left(\frac{hv - E_g}{E_u}\right) \tag{16}$$

where α is absorption coefficient, α_0 is a constant, E_g is the optical band gap, hv is the photon energy of the incident light.

The calculation of carrier lifetime

The carrier lifetime values are obtained by using the biexponential equation [8]:

$$Y = A_1 \exp\left(-\frac{t}{\tau_1}\right) + A_2 \exp\left(-\frac{t}{\tau_2}\right) \tag{17}$$

where τ_1 and τ_2 denote the fast and slow decay time and are related to the trap-assisted non-radiative and radiative recombination processes respectively, A_1 and A_2 are scaling parameters of τ_1 and τ_2 respectively. And the weighted average value τ for the lifetimes is defined by:

$$\tau = \frac{A_1\tau_1 + A_2\tau_2}{A_1 + A_2} \tag{18}$$

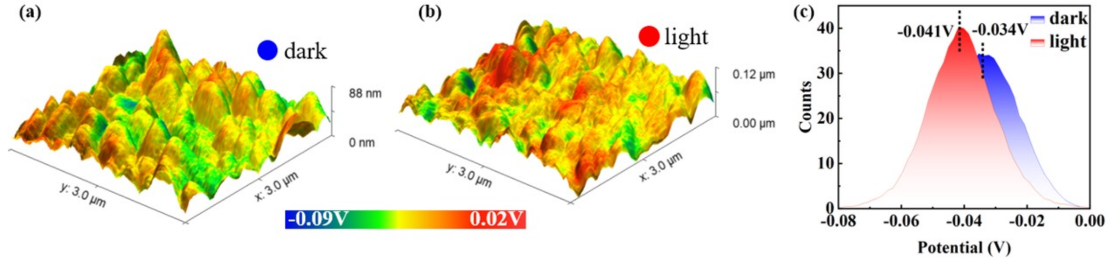

Figure S5. (a) and (b) In-situ characterization of the contact potential difference (CPD) of control sample under dark and light conditions. (c) Statistical variation of the CPD of control sample.

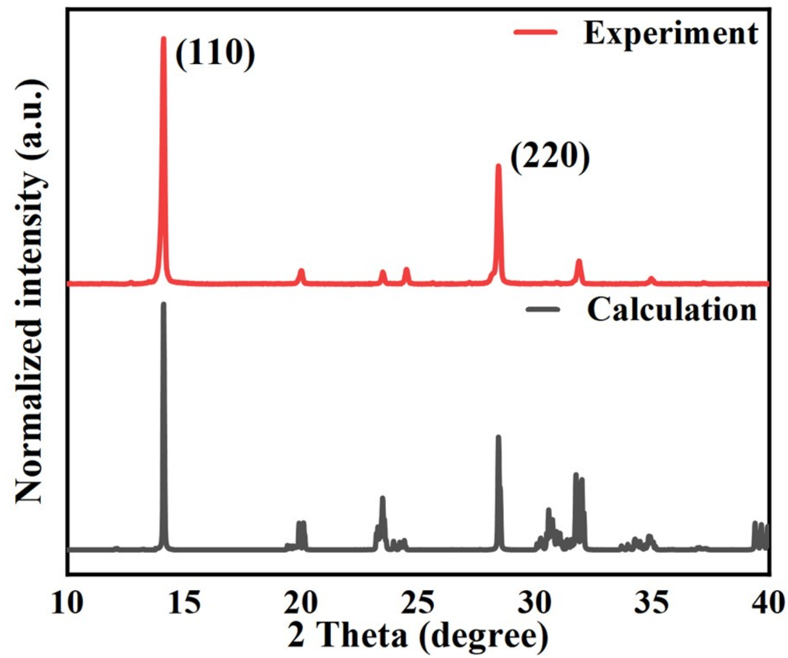

Figure S6. XRD patterns of the calculated tetragonal model and the experimental annealed sample.

Table S1. Effects of lattice strain on band gap, formation energy of defect and the effective masses of charge carriers by DFT.

Strain	Band gap (eV)	Effective mass of electron (m_0)	Effective mass of hole (m_0)	Vacancy formation energy (eV)
0.00	1.698	0.111	0.382	3.9291
0.01	1.679	0.110	0.393	3.9302
0.02	1.671	0.109	0.385	3.9321
0.03	1.655	0.108	0.378	3.9412
0.04	1.660	0.110	0.385	3.9318

References:

[1] J. Park, S. Huh, Y.W. Choi, D. Kang, M. Kim, D. Kim, S. Park, H.J. Choi, C. Kim, Y. Yi, *ACS Nano* **2024,** 18, 7570.

[2] M. Puppin, S. Polishchuk, N. Colonna, A. Crepaldi, D. Dirin, O. Nazarenko, R. De Gennaro, G. Gatti, S. Roth, T. Barillot, *Phys. Rev. Lett.* **2020,** 124, 206402.

[3] Z.-F. Li, W. Lu, G. Huang, J. Yang, L. He, S. Shen, *J. Appl. Phys.* **2001,** 90, 260.

[4] T. Pichon, S. Mouzali, O. Boulade, A. Lusson, G. Badano, J.-L. Santailler, N. Rochat, O. Gravrand, O. Limousin, *J. Electron. Mater.* **2023,** 52, 4117.

[5] F. Urbach, *Phys. Rev.* **1953,** 92, 1324.

[6] G. Cody, T. Tiedje, B. Abeles, B. Brooks, Y. Goldstein, *Phys. Rev. Lett.* **1981,** 47, 1480.

[7] V. Sa-Yakanit, H. Glyde, *Comments Cond. Mat. Phys.* **1987,** 13, 35.

[8] G. Kim, H. Min, K.S. Lee, D.Y. Lee, S.M. Yoon, S.I. Seok, *Science* **2020,** 370, 108.